Computers and Chemical Engineering 65 (2014) 18–27

Contents lists available at ScienceDirect

Computers and Chemical Engineering

journal homepage: www.elsevier.com/locate/compchemeng

Novel fluid grid and voidage calculation techniques for a discrete element model of a 3D cylindrical fluidized bed

Christopher M. Boyce[a,*], Daniel J. Holland[a], Stuart A. Scott[b], John S. Dennis[a]

[a] Department of Chemical Engineering and Biotechnology, University of Cambridge, New Museums Site, Pembroke Street, Cambridge CB2 3RA, UK
[b] Department of Engineering, University of Cambridge, Cambridge CB2 1PZ, UK

ARTICLE INFO

Article history:
Received 20 September 2013
Received in revised form 15 February 2014
Accepted 19 February 2014
Available online 28 February 2014

Keywords:
Discrete element model
Computation fluid mechanics
Fluidization
Voidage
Granular material

ABSTRACT

A discrete element model (DEM) combined with computational fluid dynamics (CFD) was developed to model particle and fluid behaviour in 3D cylindrical fluidized beds. Novel techniques were developed to (1) keep fluid cells, defined in cylindrical coordinates, at a constant volume in order to ensure the conditions for validity of the volume-averaged fluid equations were satisfied and (2) smoothly and accurately measure voidage in arbitrarily shaped fluid cells. The new technique for calculating voidage was more stable than traditional techniques, also examined in the paper, whilst remaining computationally-effective. The model was validated by quantitative comparison with experimental results from the magnetic resonance imaging of a fluidised bed analysed to give time-averaged particle velocities. Comparisons were also made between theoretical determinations of slug rise velocity in a tall bed. It was concluded that the DEM-CFD model is able to investigate aspects of the underlying physics of fluidisation not readily investigated by experiment.

1. Introduction

Fluidized beds are widely used in industry for applications ranging from fluidized catalytic cracking to drying to gasification. Additionally, fluidized beds show promise for use in chemical looping combustion of carbonaceous fuels to improve the efficiency of carbon capture. Despite the widespread industrial use, and the promise to play an important role in the supply of clean energy, the fundamental physics underpinning fluidized beds is still not fully understood.

Computational modelling provides a promising method of understanding the fundamentals of fluidisation. Currently, two forms of models predominate: discrete element modelling with computational fluid dynamics (DEM-CFD) (Hoomans, Kuipers, Briels, & Van Swaaij, 1996; Tsuji, Kawaguchi, & Tanaka, 1993) and two-fluid modelling (TFM) (Ding & Gidaspow, 1990; Kuipers, Van Duin, Van Beckum, & Van Swaaij, 1993). The main difference between DEM-CFD and TFM is that DEM-CFD treats particles as individual objects governed by Newtonian physics, while TFM considers the particles as a continuous phase governed by continuum mechanics. The main advantage of TFM over DEM-CFD is that it can model larger beds. However, DEM-CFD gives more detailed and accurate results since aspects of individual particles, such as location and velocity, can be monitored; also DEM-CFD does not require the introduction of parameters such as particle "viscosity" and "pressure". A direct comparison of DEM-CFD and TFM modelling of bubble rise in a fluidized bed, highlighting the accuracy of DEM-CFD is provided by Chiesa, Mathiesen, Melheim, and Halvorsen (2005). The paper presented here describes the development and validation of a 3D cylindrical DEM-CFD model intended to examine particular aspects of fluidization, namely pressure oscillations, particle and fluid velocity and bubble rise. Comparisons are drawn with experimental observations.

The main problem in DEM-CFD is that it does not resolve fluid flow on the sub-particle level, because the computational expense of doing so would be excessive: thus it requires a drag law to describe the fluid–particle interaction forces needed to close the equations of momentum for both phases. To account for the presence of particles in the flow field of the fluid, DEM-CFD uses a volume-averaged version of the Navier–Stokes equations for the motion of the fluid (Anderson & Jackson, 1967). These volume-averaged equations allow for the fact that a proportion of the volume of many fluid cells will be occupied by particles. The derivation of the volume-averaged equations assumes that the length scale over which the averaging takes place, equivalent to the length scale of a fluid cell, is greater than the average distance separating the centres of two neighbouring particles, but less than a distance over which macroscopic change is observed in fluid properties

* Corresponding author. Tel.: +44 07753297389.
E-mail address: cmb206@cam.ac.uk (C.M. Boyce).

http://dx.doi.org/10.1016/j.compchemeng.2014.02.019

(Anderson & Jackson, 1967). Thus, DEM-CFD cannot resolve fluid flow on a sub-particle length scale. Direct numerical simulation (DNS) could, in principle, resolve fluid flow on a sub-particle level, and thus use the no-slip boundary condition instead of a drag law to model fluid–particle interaction more accurately. However, DNS is too computationally expensive, requiring supercomputing to simulate systems of reasonable size (Xiong et al., 2012).

DEM-CFD has been a powerful tool for understanding physical phenomena in gas–solid flows. Since DEM-CFD models individual particles, it has been used to calculate particle velocity and granular temperature (He et al., 2012; Müller et al., 2008) as well as particle mixing (Bokkers, van Sint Annaland, & Kuipers, 2004; Liu, Xiao, Chen, & Bu, 2012). Additionally, since discrete element modelling can account for a variety of particle sizes, DEM-CFD has been used to model two phase granular flow in polydisperse systems of particles (Beetstra, van der Hoef, & Kuipers, 2007b; Tagami, Mujumdar, & Horio, 2009; Zeilstra, van der Hoef, & Kuipers, 2008). Since DEM-CFD can also model the flow of either liquid or gas through fluidized beds, DEM-CFD has also been able to provide insight on the differences, and transition, between homogeneous and bubbling fluidisation (Di Renzo & Di Maio, 2007).

Originally, almost all DEM-CFD simulations were limited to modelling essentially 2D fluidized beds with rectangular fluid grids, owing to computational limitations (Bokkers et al., 2004; Di Renzo & Di Maio, 2007; He et al., 2012; Liu et al., 2012; Müller et al., 2008, 2009; Tagami et al., 2009; Zeilstra et al., 2008). Since most fluidized beds used in experiments and industry have cylindrical or more complicated geometries, new DEM-CFD models for simulating beds with these geometries have recently emerged (*e.g.* Chu & Yu, 2008; Guo, Wu, & Thornton, 2013; Liu, Bu, & Chen, 2013). Fluidized beds with complicated geometries have been directly modelled using one of two techniques: (1) a rectangular fluid grid with immersed boundaries (Guo et al., 2013) or (2) an unstructured fluid grid, typically generated by a commercial CFD package (Chu & Yu, 2008). A difficulty associated with both these techniques is that it is impossible to keep the fluid cells similar in size and shape. Since the volume-averaged fluid equations (Anderson & Jackson, 1967) used in DEM-CFD models require the fluid cells to cover regions which would not change in macroscopic physical properties if slightly changed in size (Crowe, Sommerfeld, & Tsuji, 1998), having cells too small or with oblong shapes could cause these equations to break down, thereby corrupting the results. Conversely, having fluid cells too large will cause the simulation to miss important features of the flow.

Additionally, techniques involving unstructured grids require a means to determine, accurately, stably and efficiently, the void fraction in arbitrarily shaped cells. The voidage in fluid cells is defined ideally as

$$\varepsilon_{\text{cell}} = 1 - \frac{\sum V_{\text{particles}}}{V_{\text{cell}}}. \tag{1}$$

where, for the cell, $\varepsilon_{\text{cell}}$ is the voidage, $\sum V_{\text{particles}}$ the total volume of all the particles and V_{cell} is the volume. It is very important for this calculation to be accurate and stable because of the heavy dependence of certain terms in the fluid equations on voidage, especially the drag law. The calculation of voidage is complicated by the fact that particles often lie in multiple cells and it is too expensive computationally to calculate exactly the fractional particle volume lying in each cell. Mathematical equations for exactly dividing spherical particles among rectangular cells have been obtained using calculus (Freireich, Kodam, & Wassgren, 2010); however, this methodology involves expensive calculations with trigonometric functions for each particle at every time step and cannot be applied directly to fluid cells with arbitrary shapes. Wu, Zhan, Li, Lam, & Berrouk (2009) derived a complicated set of equations to calculate voidage exactly on unstructured grids, which have tetrahedral, wedge-shaped and hexahedral fluid cells. However, the method is computationally very expensive, requiring evaluations of trigonometric functions at every time step. Additionally, there is the possibility of the volume of a particle to be divided between more than ten different fluid cells, adding to the computational expense. To alleviate this computational burden, Wu et al. (2009) made a "look-up" table to solve for the volume fraction of a particle in 8×10^6 different potential positions relative to the boundaries of a fluid cell, such that the trigonometric calculations would not have to be made each time step. However, this only made a slight reduction in the computation necessary for voidage calculations, because determining the position of a particle relative to the boundaries of a fluid cell dominated the computational cost as compared to making the trigonometric calculations.

A crude method for determining voidage in any type of fluid cell, henceforth referred to as the "direct method" (also known as the "point approximation method"), would be to assume the entire volume of a particle lies in a particular fluid cell if the centre of the particle lies in that cell:

$$\varepsilon_{\text{cell}} = 1 - \sum_{i=1}^{i=N_p} \frac{V_{p,i}}{V_{\text{cell}}} \tag{2}$$

where N_p is the number of particles with centres residing in the fluid cell of interest. This calculation is obviously inexact, since a significant fraction of the volume of a particle can lie in cells other than the cell in which its centre is located. Additionally, this method could lead to instabilities because, during an individual time step, a significant fluctuation in voidage could occur if the centre of a particle moves into or out of the cell. While the direct method is the most inexpensive method computationally for structured fluid grids, in unstructured fluid grids, it can be expensive to locate the fluid cell in which the centre of each particle is located at each time step (Kuang, Yu, & Zou, 2008).

To address the issues of the direct method, a variety of other methodologies for determining voidage have been developed (Fries, Antonyuk, Heinrich, & Palzer, 2011; Khawaja, Scott, Virk, & Moatamedi, 2012; Lim, Wang, & Yu, 2006). A methodology developed by Lim et al. (2006), henceforth referred to as the "grouping method", involves calculating the voidage for a fluid cell grouped together with its surrounding cells *via* the direct method:

$$\varepsilon_{\text{cell}} = 1 - \frac{\sum_{j=1}^{N_s+1} \sum_{i=1}^{N_{p,j}} V_{p,i}}{\sum_{j=1}^{N_s+1} V_{\text{cell},j}} \tag{3}$$

where N_s is the number of cells surrounding the cell of interest and $N_{p,j}$ is the number of particles with centres which lie in fluid cell j. By including the particle volumes lying in the surrounding cells, rather than just the particle volumes in the cell of interest, this method adds stability, as large jumps in voidage do not occur when the centre of a particle moves from the cell of interest to a neighbouring cell. However, this technique adds a large amount of spatial smoothing to the averaging procedure because quantities such as velocity and pressure are calculated for individual cells, yet voidage is effectively calculated on a larger volume scale. This method of calculating voidage can also be inaccurate if the true voidage in a cell of interest is vastly different from the true voidage fractions in the surrounding cells, as can happen with bubbles passing through fluidized beds.

A commonly used method for calculating voidage on rectangular grids, described in full by Khawaja et al. (2012), involves treating each particle as if it is encapsulated by a cube, with side length equal to the diameter of the particle. The fraction of the volume of the cube which lies in different fluid cells is then calculated, and the corresponding fraction of the particle's volume is assigned to the

fluid cells which contain a portion of the volume of the encapsulating cube. This methodology, referred to here as the cuboid method, is imprecise in dividing particles, adding a small amount of spatial smoothing as compared to the exact equations of Freireich et al. (2010). However, the cuboid method is less computationally expensive than the exact equations. The technique also adds stability, compared with the direct method, without introducing the same amount of spatial smoothing as the grouping method. To estimate the spatial smoothing in the cuboid method, Khawaja et al. (2012) divided a single particle in every way possible around the exterior of a rectangular fluid cell and compared the volume fraction of the particle in the cell as calculated by the cuboid method and the exact method. They found that the cuboid method assigned at most 20% more of the volume of a particle to the fluid cell than the exact method. However, the cuboid method is not directly applicable to arbitrarily shaped fluid cells, because, although it is very easy to measure the fraction of a cube's volume in a rectangular fluid cell, it is very difficult in a cell with an arbitrary shape.

For fluid cells of arbitrary shape, Fries et al. (2011) represented a spherical particle as being composed of 10–20 cubes for voidage calculations and determined the voidage in a given fluid cell according to

$$\varepsilon_{\text{cell}} = 1 - \frac{\sum V_{\text{cube}}}{V_{\text{cell}}}. \tag{4}$$

Here $\sum V_{\text{cube}}$ is the total volume of cubes from various particles in the cell, and the entire volume of a cube is considered within a cell if the centre of the cube is located in that cell. While this model computes voidage relatively accurately, it is computationally expensive to locate the centres of all the cubes in fluid cells every time step, especially given the computational difficulties associated with locating individual points in unstructured fluid cells (Kuang et al., 2008).

To address the issues surrounding the calculation of voidage and the construction of fluid cells of valid volume and shape in non-rectangular fluid grids, a new methodology for modelling a cylindrical fluidized bed is presented here. In this model, fluid cells are all equal in volume and constructed in a cylindrical structured grid to ensure the cells have the proper volume and shape to produce an accurate fluid solution. Additionally, a novel method of calculating voidage in arbitrarily shaped fluid cells was developed giving accurate and stable predictions at low computational cost. The voidage technique is applicable to arbitrarily shaped fluid cells with only minor restrictions.

2. Theory: cylindrical fluidised bed model

Fluidization is modelled in this paper using a technique originally developed by Tsuji et al. (1993), which, as noted earlier, combines a discrete element model (DEM) (Cundall & Strack, 1979) to simulate particle motion with computational fluid dynamics of the volume-averaged Navier–Stokes equations derived by Anderson and Jackson (1967). The technique was adapted to model a cylindrical fluidized bed: the fluid dynamics was modelled in cylindrical coordinates while the motion of the particles was simulated in rectangular coordinates. Care was taken (i) to keep the fluid cells in cylindrical coordinates at a constant volume for volume-averaging purposes, and (ii) to ensure voidage was calculated accurately and without sudden changes between successive time-steps. Additionally, the CFD code was written for compressible flow and stepped forward in time using an explicit scheme, as only an explicit scheme with compressible fluid allows the prediction of pressure waves travelling through the system.

Table 1
Physical parameters used to model particle contacts.

Parameter	Value
Coefficient of sliding friction	0.1
Young's modulus	1.2×10^8 Pa
Poisson's ratio	0.33
Normal damping coefficient	0.02
Tangential damping coefficient	0.0001
Time step	1.25×10^{-6} s

2.1. Discrete element model

The motion of each particle in the fluidized bed was governed by a discrete element model, developed from that of Müller et al. (2009). Similar to this model, the linear and angular momenta of each particle were updated each time step using a force balance and Newton's second law. The normal contact force on each particle was determined using a Hertzian model, while the tangential contact force was determined using the model of Tsuji, Tanaka, and Ishida (1992), in which Coulomb's law is introduced to account for sliding. Contact parameters used for the DEM model are given in Table 1. Distinct from the discrete element model used in Müller et al. (2009), particles were confined by a tubular wall since a cylindrical fluidized bed was modelled instead of a rectangular one. Both particle and fluid motion were stepped forward explicitly in time using the 3rd order Adams–Bashforth scheme. The 3rd order Adams–Bashforth scheme was used to increase simulation accuracy and stability as compared with first- and second-order time stepping techniques.

2.2. Computational fluid dynamics

The fluid motion was modelled using computational fluid dynamics on a cylindrical grid, invoking volume-averaged Navier–Stokes equations (Anderson & Jackson, 1967) to account for portions of fluid cells being occupied by particles. The conservative form of the volume-averaged Navier–Stokes equations in cylindrical coordinates (given in Appendix A) were applied to cylindrical fluid control volumes using the finite volume method for discretisation. In order for all the fluid control volumes to have the same volume, the grid size in the radial direction was kept constant, but the angle subtended by control volumes decreased with increasing radial distance. The grid sizing in the vertical direction was constant throughout. An example of a horizontal cross section of a fluid grid used in this model is shown in Fig. 1, in which different colours show different fluid cells and each number indicates the angular index of a cell in its annulus. A mapping system was developed to ensure that the interfaces between all fluid cells received the appropriate dissipative, convective and mass fluxes, according to the finite volume method. In this mapping system, the fluid cells in the positive and negative radial directions, adjacent to the fluid cell under consideration, were identified, as well as the fraction of radial interfacial area these cells occupied. These identified fluid cells and fractions of radial interfacial area were then used in flux calculations.

To increase accuracy and stability in the fluid solution, the convective momentum fluxes in the axial (z) direction were determined using the 3rd order QUICK upwinding scheme (Leonard, 1979) with the SMART flux limiter (Gaskell & Lau, 1988). The convective fluxes in the radial and angular directions were determined using central differencing, as there were an insufficient number of cells in these directions to use high-order upwinding effectively. Using central differencing for discretisation in the radial and angular directions may have added instabilities, as compared to the QUICK upwinding scheme, but the model produced stable

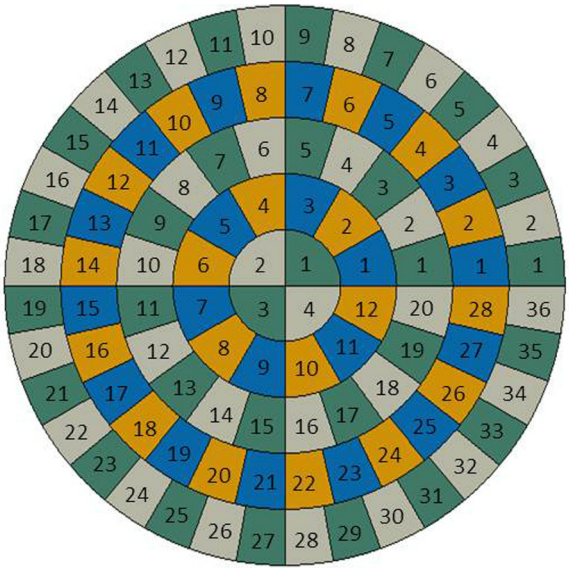

Fig. 1. Horizontal cross section of novel CFD grid. Different colours denote different CFD cells and the numbers indicate the angular index of a cell in its annulus. More CFD cells are used in the annuli further from the centre, such that the fluid cells have a constant volume to ensure the same accuracy in the volume-averaged fluid equations.

simulations, indicating that there was sufficient numerical dissipation to prevent instabilities.

The boundary conditions and other conditions used in the CFD model are summarised in Table 2. Full-slip boundary conditions were used at the cylindrical walls, because the volume-averaged Navier–Stokes equations did not allow a grid fine enough to discern the boundary layer characteristic of no-slip boundary conditions (Müller et al., 2009). At the axis of the cylinder, the velocity of the fluid was interpolated from the radial and angular velocities in the cells in the central annulus by converting these velocities into rectangular (x and y) coordinates and averaging them. At the distributor, *i.e.* the inlet for the fluid, the radial and angular velocities were set to zero. The density in these inlet cells located just below the distributor was extrapolated from the corresponding cells in the next layer up, and the inlet velocity was uniform to match that of a porous or perforated distributor with a sufficient pressure drop. At the start of the simulation, the vertical velocity of the gas at the inlet was ramped from zero to the desired value for the particular simulation over a 240 ms time period. The ramp time was chosen to be long enough to avoid long-lasting start-up effects, yet short enough to minimise simulation time. At the outlet from the bed, a three-dimensional characteristic outlet condition for isothermal flow in cylindrical coordinates was derived using the guidelines of Chung (2010), invoked as a non-reflecting boundary condition on the rate of density change at the outlet to ensure pressure waves would not be reflected back into the system. The characteristic outlet condition for change in fluid density was:

$$\Delta\rho\big|_{N_z} = \frac{\sigma_1\sigma_2}{\sigma_3}\,\Delta(\rho U_z)\big|_{N_z} \tag{5}$$

where $\Delta\rho\big|_{N_z}$ and $\Delta(\rho U_z)\big|_{N_z}$ are the change in fluid density and vertical momentum over a time step in a cell located at the outlet, N_z, and the derived constants are:

$$\begin{aligned}
\sigma_1 &= U_z^5 + U_z^4 a - 2U_z^3 a^2 - 2U_z^2 a^3 + U_z a^4 + a^5\\
\sigma_2 &= U_z^5 - U_z^4 a - 2U_z^3 a^2 + 2U_z^2 a^3 + U_z a^4 - a^5\\
\sigma_3 &= \sigma_2\sigma_5 + \sigma_6\sigma_5\\
\sigma_5 &= U_z^6 - 3U_z^4 a^2 + 2U_z^2 a^4 - a^6\\
\sigma_6 &= 2U_z^4 a - 4U_z^2 a^3 + 2a^5
\end{aligned} \tag{6}$$

where U_z is the vertical velocity in a fluid cell at the outlet and a is the isothermal speed of sound in the fluid. To complete the non-reflecting boundary condition, the changes in fluid momentum in all three directions at the outlet were extrapolated from the cell below:

$$\begin{aligned}
\Delta(\rho U_r)\big|_{N_z} &= \Delta(\rho U_r)\big|_{N_{z-1}}\\
\Delta(\rho U_\theta)\big|_{N_z} &= \Delta(\rho U_\theta)\big|_{N_{z-1}}\\
\Delta(\rho U_z)\big|_{N_z} &= \Delta(\rho U_z)\big|_{N_{z-1}}
\end{aligned} \tag{7}$$

2.3. Linkage between fluid and particles

The linkage between fluid and particles was accounted for (1) in the calculation of voidage for each fluid control volume and (2) in the fluid–particle interaction force. Determining voidage in each cylindrical fluid cell requires a balance between smoothness and accuracy to achieve an accurate and stable simulation. Therefore, a technique, referred to as the "square grid method", was developed for determining voidage in arbitrarily-shaped fluid cells. Here, the distribution of particle volume on a square grid was calculated and mapped on to the cylindrical control volumes to calculate voidage, as depicted in Fig. 2. To do this, firstly the geometric fraction of the volume of each of the box-shaped cells which lies in each of the cylindrical control volumes was calculated. During every time step, the volume of particles in each box-shaped cell was calculated, utilising the cuboid approximation described earlier for smoothly determining the volume fraction of particles which lie in multiple rectangular cells (Khawaja et al., 2012). These particle volumes were then translated to the cylindrical control volumes using the pre-calculated geometric fractions to calculate the volume of particles in each fluid control volume. This calculation is summarised in Eq. (8):

$$\begin{aligned}
V_{p,\mathrm{tot,cylindrical}}(r,\theta) = \sum_l \sum_m (&\mathrm{VolFrac}(l,m,r,\theta)\\
&\cdot V_{p,\mathrm{tot,Cartesian}}(l,m)).
\end{aligned} \tag{8}$$

in which $V_{p,\mathrm{tot,Cartesian}}(l,m)$ is the volume of particles in box (l,m), $V_{p,\mathrm{tot,cylindrical}}(r,\theta)$ is the volume of particles in the cylindrical fluid control volume (r,θ) and $\mathrm{VolFrac}(l,m,r,\theta)$ is the fraction of volume of box (l,m) taken up by control volume (r,θ). Finally these volumes of particles were used to calculate the voidage, $\varepsilon(r,\theta)$, in each fluid control volume, using

$$\varepsilon(r,\theta) = 1 - \frac{V_{p,\mathrm{tot,cylindrical}}(r,\theta)}{V_{\mathrm{cell}}}. \tag{9}$$

where V_{cell} is the volume of the cylindrical control volume. The square grid method has an obvious source of inaccuracy in that a fraction of the volume of a particle can be registered as being in a

Table 2
Boundary and other simulation conditions used to model fluid motion.

Aspect of Simulation	Condition Imposed
Fluid–particle interaction	Beetstra, van der Hoef, and Kuipers (2007a, 2007b) Correlation
Fluid type	Compressible
Time stepping scheme	Explicit 3rd order Adams–Bashforth
Inlet voidage	0.4
Outlet condition	3D cylindrical characteristic outlet
Boundary velocity	Full-slip

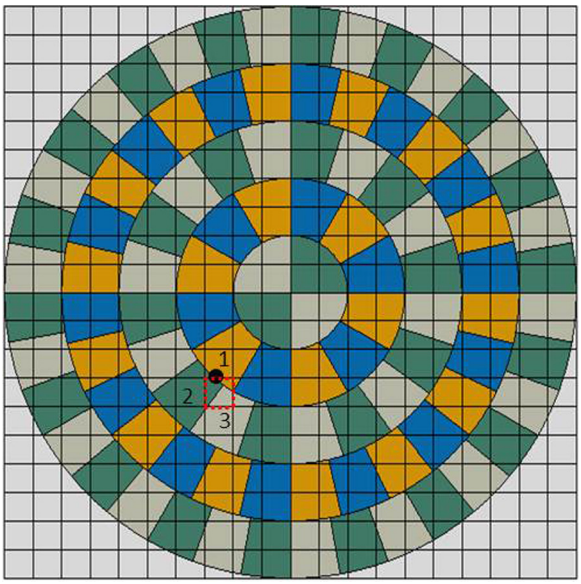

Fig. 2. Voidage calculation method. The particle depicted lies in two box cells, so its volume is divided between both of them using the cuboid approximation (Khawaja, Scott, Virk, & Moatamedi, 2012). Since box cell outlined in red has portions of its volume in fluid cells "1", "2" and "3", a portion of the particle's volume is counted as being fluid cell "3", even though none of its actual volume is in this cell.

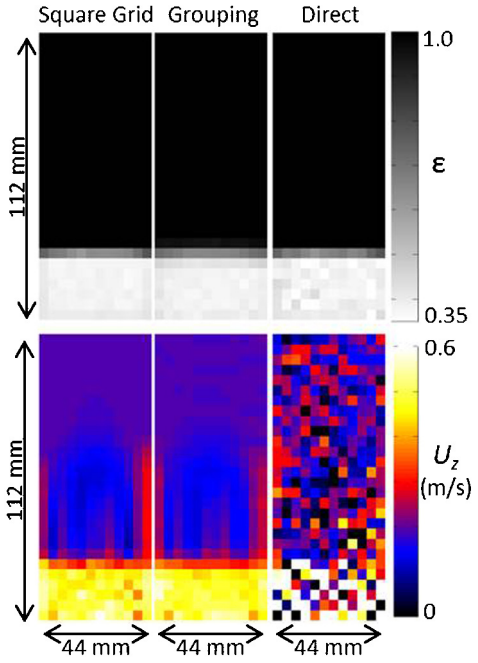

Fig. 3. Comparison of voidage calculation methods for packed bed flow. Comparison of the square grid, grouping and direct calculation methods for voidage (top) and vertical fluid velocity (bottom) measurements in packed bed flow. The fluid grid used is described in Setup 2 in Table 3.

control volume in which the particle is not located. This can be seen in Fig. 2, where a particle, shown as a black circle, has its volume divided between an upper and lower square box. The volume of the upper box is divided between the fluid cells denoted "1" and "2", and the volume of the lower box, highlighted in red, is divided among cells "1", "2" and "3". Thus, a small portion of the volume of the particle is assigned to cell "3", even though none of its volume actually lies in cell "3". Hence, the square grid method involves some of the spatial smoothing inherent in the grouping method, but to a lesser extent. This technique, however, provides stability by taking advantage of the stability inherent in the cuboid approximation developed for rectangular grids. Additionally, this method is computationally efficient because the computationally-expensive calculations only take place during initialisation. The square grid method would thus provide a distinct advantage in computational efficiency when applied to unstructured grids, because the unstructured fluid cell in which particle centres, or cube fractions of particles (given by Eq. (4)), lie would not have to be identified every time step. To provide a comparison, the cylindrical model was also run with the direct and grouping voidage calculation techniques.

The interaction force between fluid and particles was modelled using the drag law developed by Beetstra et al. (2007b). This drag law was chosen because it matched experimental results better than other drag laws when used in a previous discrete element model of a fluidized bed (Müller et al., 2009); however, recent work has suggested that further improvements may be required for an accurate model of drag force (Kriebitzsch, van der Hoef, & Kuipers, 2013). In order to obtain the relative velocity between the fluid and particles, the radial and angular velocities of the fluid were converted to rectangular velocities at the position of the particle of interest. After the interaction force was calculated for a particle in rectangular coordinates, this force was converted into cylindrical coordinates and added to the cumulative interaction force on the fluid cell in which the centre of the particle was located. The fluid–particle interaction force was not divided between fluid cells, since this would require much more computational time than dividing the particle volume between fluid cells. Additionally, since drag force is not imparted equally on a particle by fluid in all directions relative to the centre of the particle, it was expected that having the interaction force based on the velocity of fluid in the cell where the centre of the particle was located would model the interaction force relatively well.

3. Results

3.1. Comparison of voidage calculation techniques

Fig. 3 compares the three techniques for voidage calculation for simulating steady flow of gas through a packed bed. All techniques give approximately the same overall voidage, although that given by the direct method appears to be the least smoothed spatially. The square grid and grouping methods give very similar patterns of vertical flow of fluid, with the highest velocities in the packed bed region and lowest velocities in the freeboard. The direct method, however, gives non-physical results for vertical velocity, showing extreme, non-physical jumps in velocity between adjacent fluid cells; indeed, the result for the direct method was so unstable that the simulation failed to reach a final solution during the modelling of steady flow in a packed bed. Fig. 3 demonstrates that a technique for calculating voidage must have a smooth transition in the voidage calculated for a particular cell as the centres of particles move into and out of that cell. In packed bed flow, particles barely move, yet even small motions are capable of providing non-physical fluid flow results in the direct method. Thus, the direct method was not considered for modelling fluidized beds. The stability provided by spatial smoothing for the grouping method, and division of particles among square cells in the square grid method, allows these two techniques to give stable results for flow of fluid in a packed bed.

Fig. 4 compares techniques for calculating voidage when simulating bubbling fluidization. The instantaneous vertical fluid velocity and voidage predicted by the square grid and grouping methods are compared for a situation in which a bubble is reaching the top of the bed. Additionally, Fig. 4 compares the time-averaged voidage and vertical fluid velocity predicted by both techniques, averaged over a period of 2.1 s. Both techniques give similar results

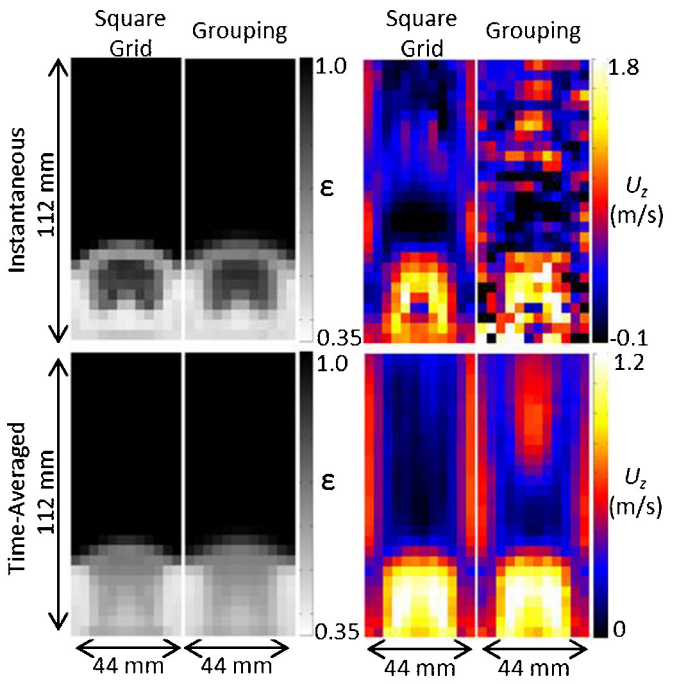

Fig. 4. Comparison of voidage calculation methods for modelling a bubbling fluidized bed. This figure provides a comparison of the square grid and grouping voidage calculation methods on the basis of voidage and vertical fluid velocity for instantaneous (top) and time-averaged (bottom) flow. For instantaneous flow, a characteristic image of flow as a bubble reaches the surface of the bed is shown. For time-averaged flow, the voidage and vertical fluid velocity were averaged over 2.1 s, during which time 17 bubbles passed through the system. The fluid grid used is described in Setup 2 in Table 3.

for instantaneous and time-averaged voidage. However, the grouping method does providing more spatial smoothing, as can be seen by the lesser contrast predicted between the voidage in the interior of the bubble and the voidage at the edges of the bubble. For instantaneous predictions of the velocity of the fluid, the square grid method gives the expected result for bubbling fluidization. It would be expected that nearly all fluid flow is directed through the bubble with almost no flow around the sides of the bubble, due to the low resistance to fluid flow due to drag force in the bubble. With a superficial gas velocity of 0.60 m/s and the horizontal cross section of the bubble taking up approximately 40% of the bed, the flow through the bubble could be expected to be roughly 1.5 m/s. In Fig. 4a, fluid is moving fastest through the bubble, at roughly 1.5 m/s, and much slower, nearly zero, around the outskirts of the bubble. The grouping method, however, produces non-physical instantaneous fluid velocity results, with large changes in fluid velocity between adjacent fluid cells. Both methods give similar, physically-sensible results for time-averaged vertical fluid velocity in the bed region, yet the grouping method gives a non-physical increase in velocity towards the top of the freeboard in the centre of the bed. This non-physical increase further emphasises the superiority of the square grid method over the grouping method in simulating bubbling fluidization.

Fig. 4 shows that stability is even more important for simulating bubbling fluidization than packed bed flow, since particles move between fluid cells rapidly. In this case, the spatial smoothing provided by the grouping method no longer provides enough stability to give physically-sensible images of instantaneous fluid velocity. For bubbling fluidization, physically-sensible instantaneous fluid velocities are only achieved by the technique of dividing particle volumes between fluid cells provided by the square grid method.

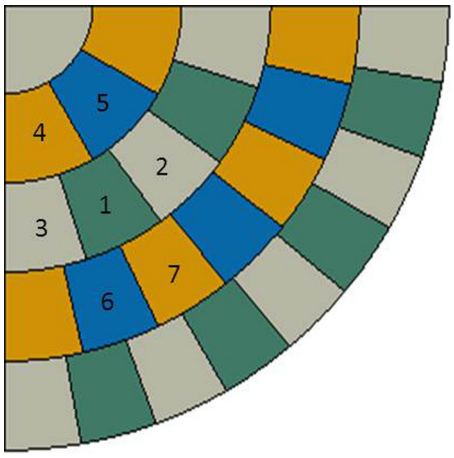

Fig. 5. Fluid cell notation for a comparison of voidage method calculations with the entire volume of all particles residing in fluid cell 1. Fluid cells 8 and 9 are vertically below and above fluid cell 1, respectively.

3.2. Comparison of spatial smoothing provided by various voidage calculation techniques

The spatial smoothing provided by the direct, grouping and square-grid methods of calculating voidage was compared by assessing the voidage calculated on a grid with a randomly-packed set of particles using each technique. The set of 26 particles was selected such that the entire volume of every particle resided in the same fluid cell, denoted "1" in Fig. 5. Thus, an ideal calculation of voidage would determine the voidage to be unity ($\varepsilon = 1$) in every other cell. In addition to comparing the direct and grouping techniques, three different sizes of the square grid were compared. In each square grid, the length of the grid cells in the vertical direction (dl_z) was kept constant and equal to length (dz) of the fluid grid cells in the vertical direction ($dl_z = dz$). However, the length of the voidage cells in the horizontal direction ($dl_{x,y}$) was varied as follows. Configuration 1 had side length equal to the length (dr) of the fluid cells in the radial direction ($dl_{x,y} = dr = 4.4$ mm). Configuration 2 had side length half that of the fluid cells in the radial direction ($dl_{x,y} = 0.5dr = 2.2$ mm) and configuration 3 had side length just larger than the diameter of the particles ($dl_{x,y} = 1.375$ mm; $d_p = 1.2$ mm). The square grid voidage was calculated using both the cuboid approximation described by Khawaja et al. (2012) to divide particles amongst square cells as well as the exact formulae for dividing particles amongst square cells, derived by Freireich et al. (2010).

The voidage calculated in the various cells denoted in Fig. 5 for each voidage technique is shown in Table 3. Fluid cells 8 and 9 refer to the cells vertically below and above fluid cell 1, respectively. In this example, the voidage calculated by the direct method gave $\varepsilon = 0.692$ in cell 1 and $\varepsilon = 1$ in all other cells and is exact, because the entire volume of all 26 particles resides in cell 1. However, it is important to note that in most cases, where particles are divided among multiple fluid cells, the direct method would not provide an exact calculation of voidage. The grouping method provides the most spatial smoothing, since the voidage in cell 1 is the closest to unity and the voidage in all other cells is the furthest from unity of all of the techniques. In fact, fluid cells 1, 2, 3, 8 and 9 all have the same voidage for this example using the grouping method, because they all share a full interface. As expected, the voidage calculated using the square grid method has increased accuracy and with a finer square grid in the horizontal direction, since voidage grid cells span fewer fluid grid cells. Even the very coarse voidage grid of configuration 1 provides slightly less spatial smoothing than the grouping method since its voidage

Table 3
Voidage measured in various fluid cells using the direct, grouping and square grid methods. Fig. 5 provides a diagram of the location of the different fluid cells. The entire volume of all particles in this example resides in fluid cell 1. Square grid length in the horizontal direction decreases with increasing configuration number. The square grid calculation is made using both the cuboid approximation and the exact equations to calculate the division of particles amongst box cells.

Fluid cell	Voidage calculated using:							
	Direct method	Grouping method	Square grid with cuboid approximation			Square grid with exact division of particles amongst square cells		
			Config. 1	Config. 2	Config. 3	Config. 1	Config. 2	Config. 3
1	0.692	0.956	0.907	0.796	0.755	0.907	0.795	0.752
2	1	0.956	0.949	0.966	0.971	0.949	0.966	0.972
3	1	0.956	0.940	0.962	0.978	0.938	0.961	0.977
4	1	0.982	0.995	0.997	0.999	0.998	0.998	0.999
5	1	0.991	0.981	0.991	0.996	0.981	0.991	0.997
6	1	0.974	0.982	0.990	0.998	0.982	0.991	0.998
7	1	0.965	0.947	0.992	0.995	0.948	0.993	0.997
8	1	0.956	1	1	1	1	1	1
9	1	0.956	1	1	1	1	1	1

measurement in cell 1 is further from unity. The voidage calculated by the square grid with exact division of particles amongst square cells is essentially the same as that calculated using the square grid method with the cuboid approximations, showing that use of the cuboid method does not provide much excess spatial smoothing. In all square grid techniques in this example, there is no spatial smoothing in the vertical direction ($\varepsilon = 1$ for cells 8 and 9) because the voidage grid is aligned with the fluid grid in the vertical direction. If a particle did cross the vertical boundaries of the fluid cells, its volume would be divided between those cells fairly accurately, either using the cuboid approximation or the exact calculation. The minimal smoothing in the vertical direction is important for accurate simulation in fluidized beds, since the largest difference between adjacent cells in voidage and flow field is often in the vertical direction.

3.3. Grid size for the square grid voidage technique

To simulate bubbling fluidization in a short bed, three sizes of square grid for calculating voidage were used, in order to assess the effect of grid size on the results. The three configurations of square grid are the same as those described in Section 3.2. The system had $d_p = 1.2$ mm particles, a bed diameter of $D_{bed} = 44$ mm and a tapped bed height of 30 mm. Fig. 6 shows the predicted time-averaged voidage, fluid velocity and vertical particle velocities for the three sizes. The time-averaged results are very similar and investigation of the instantaneous results also showed essentially no difference among the three simulations. This similarity indicates that the extra spatial smoothing provided by coarser square grids demonstrated in Section 3.2, has minimal effect on the simulated results for a short bubbling bed. However, other configurations of granular systems with more abrupt spatial changes in voidage, such as jetting and spouted beds, might require finer square grids for accurate results. Additionally, the three simulations all took about the same amount of time to run, since computational expense was dominated by the particle contact calculations, rather than voidage calculations. Thus, it is probably better to use fine voidage grids, with side length just greater than the diameter of the particles, to ensure accuracy without compromising speed for most granular system configurations.

3.4. Simulating bubbling and slugging fluidized beds with DEM-CFD model: comparison with experiments

The DEM-CFD model was used to simulate bubbling fluidization in a short bed. Fig. 7 shows a comparison of time-averaged particle velocity between the experimental magnetic resonance (MR) measurements of Holland, Müller, Dennis, Gladden, and Sederman (2008) and predictions from the cylindrical DEM-CFD model. The raw DEM-CFD results were processed using a particle-based average, as described by Boyce, Holland, Scott, and Dennis (2013), in order to match the MR averaging procedure. The bed modelled was the same as that described in Section 3.3 and used experimentally by Holland et al. (2008). The square grid used to calculate local voidage was arranged in configuration 3, described in Section 3.2. The maps of velocities are similar in profile and magnitude, thereby validating the DEM-CFD model.

Next, a tall, slugging fluidized bed was simulated in order to investigate the slug rise velocity predicted by the DEM-CFD model. A bed was modelled with particles of $d_p = 1.2$ mm, a bed diameter of $D_{bed} = 50$ mm and a tapped bed height of 160 mm. This bed was fluidized at superficial velocities of $U = 0.37$, 0.425, 0.54 and

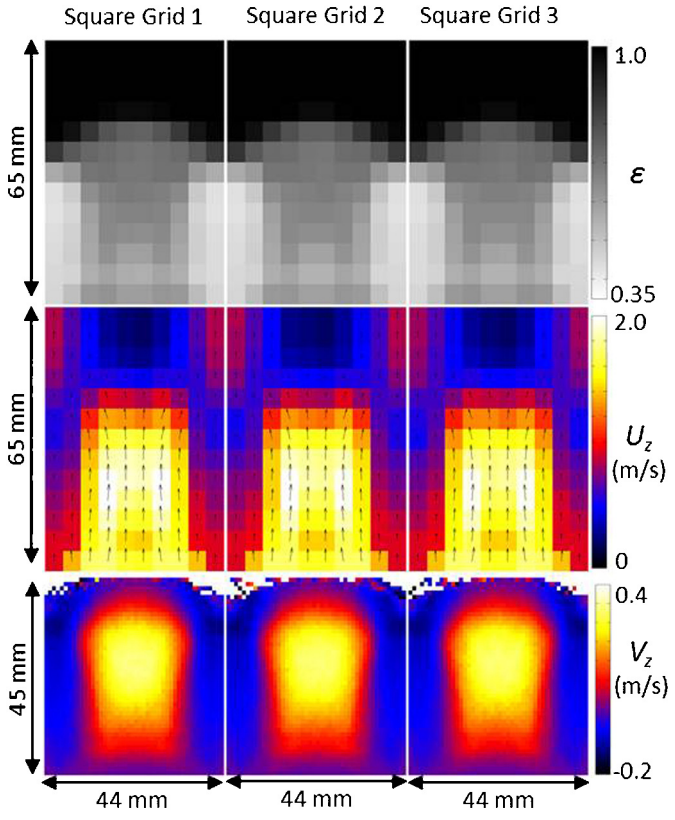

Fig. 6. Comparison of time averaged voidage (top), fluid velocity (middle) and vertical particle velocity (bottom) for a short bubbling bed with decreasing size of the square grid used for calculating voidage.

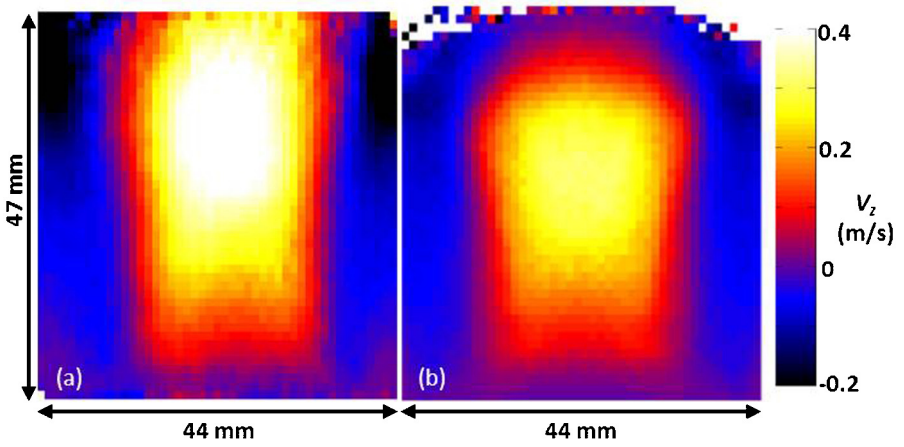

Fig. 7. Validation of 3D cylindrical model *via* comparison of time-average axial particle velocity images from: (a) experimental MR imaging and (b) DEM-CFD simulation of a bubbling fluidized bed. The bed was fluidized at U/U_{mf} = 2 and had a settled height of 30 mm with particles 1.2 mm in diameter. The field of view for each image is 47 mm (z) by 44 mm (x) and the resolution is 1.04 mm (z) by 0.94 mm (x).

0.60 m/s, with U_{mf} = 0.30 m/s determined experimentally by Müller et al. (2007a) and confirmed by DEM-CFD simulations in which U was slowly decreased from above U_{mf} until the pressure drop across the bed began to decrease. In the simulations, bubbles formed at the distributor and then grew and coalesced with one another until fully formed axisymmetric slugs rose from approximately 120 mm above the distributor and upwards. A theoretical rise velocity for axisymmetric slugs in fluidized beds was derived by Stewart and Davidson (1967):

$$U_S = U - U_{mf} + 0.35\sqrt{gD_{\text{bed}}} \tag{10}$$

The average slug rise velocity predicted by the DEM-CFD simulations with different superficial velocities was calculated using the cross-correlation method of Müller et al. (2007a). The average rise velocity of fully formed slugs 140 mm above the distributor calculated over 4.2 s of steady slugging is shown in Fig. 8, and compared to the theory of Stewart and Davidson (1967). The DEM-CFD predictions match those predicted by Eq. (10) very well. DEM-CFD

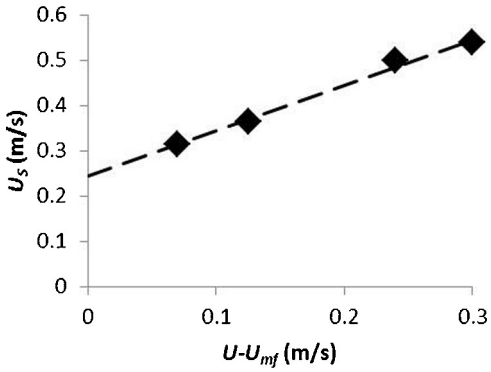

Fig. 8. DEM-CFD simulation predictions for slug rise velocity (U_S) for simulations with different superficial velocities (U) above the minimum fluidization velocity (U_{mf}). Simulation predictions (♦) are compared to the theoretical rise velocity of axisymmetric slugs (- - -) (Stewart & Davidson, 1967). A bed 50 mm in diameter was simulated, filled to a settled bed height of 160 mm with seed 1.2 mm in diameter with a minimum fluidization velocity of 0.30 m/s. Rise velocities of slugs were measured 140 mm above the distributor and averaged over 4.2 s of steady slugging.

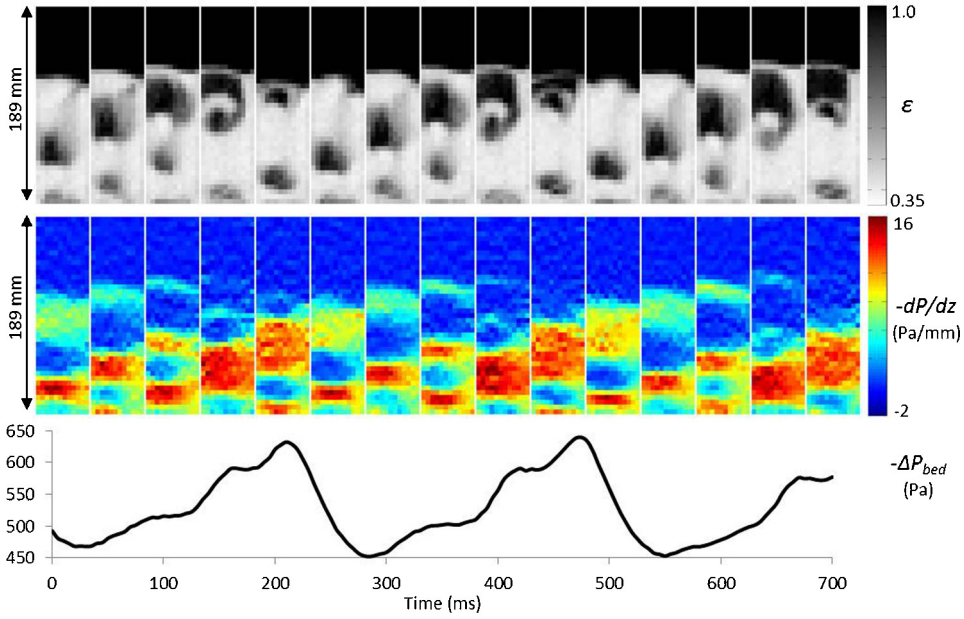

Fig. 9. Use of the cylindrical DEM-CFD model to analyse the origins of pressure fluctuations in bubbling fluidized beds. The top row shows a series of voidage maps taken every 50 ms in a 50 mm diameter bed; the middle and bottom rows show the corresponding maps of pressure drop per unit vertical distance and total pressure drop across the bed, respectively.

predictions also show that the quantity $(U - U_{mf})$ must be included in the equation for slug rise velocity, in keeping with the two-phase theory of fluidization (Davidson & Harrison, 1963) and matching a conclusion of experimental studies of slug rise velocity by Müller et al. (2007a), undertaken on a taller bed.

Thus far, the combination of the above comparisons between theory and experiment suggests that the cylindrical model is promising for predicting various properties of bubbling and slugging fluidized beds. To take the use of the DEM-CFD model a step further, the origin of the oscillations in pressure drop across a slugging fluidised bed was investigated. Fig. 9 shows a series of voidage maps over time, with bubbles coalescing and a wall slug rising in the simulated fluidized bed. In this case, a 50 mm wide bed was used, filled with particles 1.2 mm in diameter to a tapped height of 110 mm. The bed was fluidized at a superficial velocity of $U = 0.563$ m/s. In addition to calculating voidage, Fig. 9 shows the ability of the DEM-CFD to map differential pressure drop in the z-direction as well as overall pressure drop over time. The plots of voidage and pressure drop over time show that the period of oscillations in pressure drop matches the period of time taken for a pair of bubbles to erupt at the top of the bed in quick succession, consistent with the experimental results of Müller et al. (2007b). From the simulations, it can be seen that pressure drop across the system reaches a maximum after a large bubble followed by a smaller bubble erupt in quick succession, leaving a tall plug of particles behind them at the top of the bed. There is a large local pressure drop in this plug, inducing the maximum overall pressure drop. In contrast, the pressure drop reaches a minimum when only a single large bubble is rising through the system because essentially no pressure drop across the bubble. These insights show the ability of the model developed here, using an explicit scheme to account for the ability of pressure waves to propagate, to investigate the interaction of bubble passage and pressure fluctuations in more detail than has hitherto been possible.

4. Conclusions

The DEM-CFD model developed provides an important tool for modelling 3D cylindrical fluidized beds with a high level of control over fluid grid sizing, which ensures that the conditions for using volume-averaged fluid equations will be satisfied, whilst allowing the fluid grid size to be fine enough in all regions so as to not miss key flow features. The model was validated by comparison with experimental MR results and well-established theory for bubbling and slugging beds of various heights.

The square grid methodology developed for calculating voidage proved an effective way for accurately and stably measuring voidage in arbitrarily-shaped control volumes. The technique proved more stable than the direct method and more accurate spatially than the grouping method. In this paper, the square grid technique was used on a structured, cylindrical fluid grid, but it could be applied to unstructured grids. In order to use the square grid method on an unstructured grid, the volume fraction of square voidage grid cells which lies in the unstructured fluid grid cells would have to be calculated. This calculation would be complicated, because it requires locating the faces of fluid grid cells in a rectangular coordinate system and numerically integrating to determine overlapping volumes between the voidage and fluid grid cells. However, this process would only need to be conducted at the start of a simulation, after which the computationally-inexpensive calculations of voidage on a square grid, and translating that voidage to an unstructured grid, could be conducted to determine voidage at every time step. Thus, the square grid voidage technique is probably less expensive computationally for unstructured fluid grids than the direct and grouping methods, as well as the method approximating the shape of a sphere as a set of cubes. With regard to accuracy and stability for unstructured fluid grids, the square grid method would provide the same benefits over the direct and grouping methods described in this paper.

Acknowledgments

CMB would like to acknowledge the financial support of the Gates Cambridge Trust. DJH would like to acknowledge the financial support of the EPSRC (Grant no. EP/K008218/1).

Appendix A. Fluid equations in cylindrical coordinates

In order to simulate a cylindrical geometry, the CFD code developed here used the conservative form of the volume averaged Navier–Stokes equations (Anderson & Jackson, 1967) in cylindrical coordinates:

$$\frac{\partial \boldsymbol{F}}{\partial t} + \frac{1}{r}\frac{\partial}{\partial r}(r\boldsymbol{C}_r) + \frac{1}{r}\frac{\partial \boldsymbol{C}_\theta}{\partial \theta} + \frac{\partial \boldsymbol{C}_z}{\partial z} = \frac{\varepsilon}{r}\frac{\partial}{\partial r}(r\boldsymbol{D}_r) + \frac{\varepsilon}{r}\frac{\partial \boldsymbol{D}_\theta}{\partial \theta} + \varepsilon\frac{\partial \boldsymbol{D}_z}{\partial z} + \boldsymbol{S} + \boldsymbol{g} + \boldsymbol{I} \tag{A.1}$$

where ε is the local volume-averaged voidage and the bold letters are column vectors consisting of 4 rows, denoting the (1) continuity, (2) radial momentum, (3) angular momentum and (4) axial momentum equations. The $\boldsymbol{F}$ matrix represents required conserved quantities, thus:

$$\mathbf{F} = \begin{bmatrix} \rho\varepsilon \\ \rho\varepsilon U_r \\ \rho\varepsilon U_\theta \\ \rho\varepsilon U_z \end{bmatrix} \tag{A.2}$$

where ρ is the local volume-averaged fluid density, and U_r, U_θ, and U_z are the radial, angular and axial components of the local volume-averaged fluid velocity vector, respectively. The $\boldsymbol{C}_r$, $\boldsymbol{C}_\theta$, and $\boldsymbol{C}_z$ matrices represent the convective flux matrices in the radial, angular and axial directions:

$$\boldsymbol{C}_r = \begin{bmatrix} \rho\varepsilon U_r \\ \rho\varepsilon U_r U_r \\ \rho\varepsilon U_\theta U_r \\ \rho\varepsilon U_z U_r \end{bmatrix} \quad \boldsymbol{C}_\theta = \begin{bmatrix} \rho\varepsilon U_\theta \\ \rho\varepsilon U_r U_\theta \\ \rho\varepsilon U_\theta U_\theta \\ \rho\varepsilon U_z U_\theta \end{bmatrix} \quad \boldsymbol{C}_z = \begin{bmatrix} \rho\varepsilon U_z \\ \rho\varepsilon U_r U_z \\ \rho\varepsilon U_\theta U_z \\ \rho\varepsilon U_z U_z \end{bmatrix} \tag{A.3}$$

The $\boldsymbol{D}_r$, $\boldsymbol{D}_\theta$, and $\boldsymbol{D}_z$ matrices represent the diffusive flux matrices in the radial, angular and axial directions:

$$\boldsymbol{D}_r = \begin{bmatrix} 0 \\ \tau_{rr} - P \\ \tau_{r\theta} \\ \tau_{rz} \end{bmatrix} \quad \boldsymbol{D}_\theta = \begin{bmatrix} 0 \\ \tau_{\theta r} \\ \tau_{\theta\theta} - P \\ \tau_{\theta z} \end{bmatrix} \quad \boldsymbol{D}_z = \begin{bmatrix} 0 \\ \tau_{zr} \\ \tau_{z\theta} \\ \tau_{zz} - P \end{bmatrix} \tag{A.4}$$

where P is local volume averaged pressure, and τ is the nine-component stress tensor, in which the first subscript denotes which direction momentum is diffusing in and the second subscript denotes which component of momentum is diffusing. The differential forms of the stress tensor components are:

$$\tau_{rr} = 2\mu\frac{\partial U_r}{\partial r} + \left(L - \frac{2}{3}\mu\right)(\nabla \cdot \boldsymbol{U}) \tag{A.5}$$

$$\tau_{\theta\theta} = 2\mu\left(\frac{1}{r}\frac{\partial U_\theta}{\partial \theta} + \frac{U_r}{r}\right) + \left(L - \frac{2}{3}\mu\right)(\nabla \cdot \boldsymbol{U}) \tag{A.6}$$

$$\tau_{zz} = 2\mu\frac{\partial U_z}{\partial z} + \left(L - \frac{2}{3}\mu\right)(\nabla \cdot \boldsymbol{U}) \tag{A.7}$$

$$\tau_{r\theta} = \tau_{\theta r} = \mu\left(r\frac{\partial}{\partial r}\left(\frac{U_\theta}{r}\right) + \frac{1}{r}\frac{\partial U_r}{\partial \theta}\right) \tag{A.8}$$

$$\tau_{\theta z} = \tau_{z\theta} = \mu\left(\frac{\partial U_\theta}{\partial z} + \frac{1}{r}\frac{\partial U_z}{\partial \theta}\right) \tag{A.9}$$

$$\tau_{rz} = \tau_{zr} = \mu\left(\frac{\partial U_z}{\partial r} + \frac{\partial U_r}{\partial z}\right) \tag{A.10}$$

where μ and L are the viscosity and bulk viscosity, respectively and $\nabla \cdot \boldsymbol{U}$ is the divergence:

$$\nabla \cdot \boldsymbol{U} = \frac{1}{r}\frac{\partial}{\partial r}(rU_r) + \frac{1}{r}\frac{\partial U_\theta}{\partial \theta} + \frac{\partial U_z}{\partial z} \tag{A.11}$$

which is calculated using the finite volume method. The $\boldsymbol{S}$, $\boldsymbol{g}$ and $\boldsymbol{I}$ matrices denote the source components due to aspects of the cylindrical inertial reference frame, gravity and fluid–particle interaction, respectively:

$$\boldsymbol{S} = \begin{bmatrix} 0 \\ \rho U_\theta U_\theta/r - \tau_{\theta\theta}/r \\ -\rho U_r U_\theta/r + \tau_{\theta r}/r \\ 0 \end{bmatrix} \quad \boldsymbol{g} = \begin{bmatrix} 0 \\ 0 \\ 0 \\ -9.81 \end{bmatrix} \quad \boldsymbol{I} = \begin{bmatrix} 0 \\ I_r \\ I_\theta \\ I_z \end{bmatrix} \tag{A.12}$$

where the stress components in $\tau_{\theta\theta}$ and $\tau_{\theta r}$ act on the centre of the fluid control volumes rather than the faces and I_r, I_r and I_r represent the radial, angular and axial components of the local volume-averaged fluid–particle interaction force.

References

Anderson, T. B., & Jackson, R. (1967). Fluid mechanical description of fluidized beds. *Industrial and Engineering Chemistry Fundamentals*, *6*(4), 527–539.

Beetstra, R., van der Hoef, M. A., & Kuipers, J. A. M. (2007a). Drag force of intermediate Reynolds number flow past mono- and bidisperse arrays of spheres. *AIChE Journal*, *53*(2), 489–501. http://dx.doi.org/10.1002/aic.11065

Beetstra, R., van der Hoef, M. A., & Kuipers, J. A. M. (2007b). Numerical study of segregation using a new drag force correlation for polydisperse systems derived from lattice-Boltzmann simulations. *Chemical Engineering Science*, *62*(1-2), 246–255. http://dx.doi.org/10.1016/j.ces.2006.08.054

Bokkers, G. A., van Sint Annaland, M., & Kuipers, J. A. M. (2004). Mixing and segregation in a bidisperse gas–solid fluidised bed: A numerical and experimental study. *Powder Technology*, *140*(3), 176–186. http://dx.doi.org/10.1016/j.powtec.2004.01.018

Boyce, C. M., Holland, D. J., Scott, S. A., & Dennis, J. S. (2013). Adapting data processing to compare model and experiment accurately: A discrete element model and magnetic resonance measurements of a 3D cylindrical fluidized bed. *Industrial and Engineering Chemistry Research*, *52*(50), 18085–18094. http://dx.doi.org/10.1021/ie401896x

Chiesa, M., Mathiesen, V., Melheim, J. A., & Halvorsen, B. (2005). Numerical simulation of particulate flow by the Eulerian–Lagrangian and the Eulerian–Eulerian approach with application to a fluidized bed. *Computers and Chemical Engineering*, *29*(2), 291–304. http://dx.doi.org/10.1016/j.compchemeng.2004.09.002

Chu, K. W., & Yu, A. B. (2008). Numerical simulation of complex particle–fluid flows. *Powder Technology*, *179*(3), 104–114. http://dx.doi.org/10.1016/j.powtec.2007.06.017

Chung, T. J. (2010). *Computational fluid dynamics*. Cambridge; New York: Cambridge University Press.

Crowe, C., Sommerfeld, M., & Tsuji, Y. (1998). *Multiphase flows of droplets and particles* (1st ed.). Boca Raton, FL: CRC Press.

Cundall, P. A., & Strack, O. D. L. (1979). A discrete numerical model for granular assemblies. *Géotechnique*, *29*(1), 47–65. http://dx.doi.org/10.1680/geot.1979.29.1.47

Davidson, J. F., & Harrison, D. (1963). *Fluidised particles*. Cambridge: Cambridge University Press.

Di Renzo, A., & Di Maio, F. P. (2007). Homogeneous and bubbling fluidization regimes in DEM–CFD simulations: Hydrodynamic stability of gas and liquid fluidized beds. *Chemical Engineering Science*, *62*(1–2), 116–130. http://dx.doi.org/10.1016/j.ces.2006.08.009

Ding, J., & Gidaspow, D. (1990). A bubbling fluidization model using kinetic theory of granular flow. *AIChE Journal*, *36*(4), 523–538. http://dx.doi.org/10.1002/aic.690360404

Freireich, B., Kodam, M., & Wassgren, C. (2010). An exact method for determining local solid fractions in discrete element method simulations. *AIChE Journal*, *56*(12), 3036–3048. http://dx.doi.org/10.1002/aic.12223

Fries, L., Antonyuk, S., Heinrich, S., & Palzer, S. (2011). DEM–CFD modeling of a fluidized bed spray granulator. *Chemical Engineering Science*, *66*(11), 2340–2355. http://dx.doi.org/10.1016/j.ces.2011.02.038

Gaskell, P. H., & Lau, A. K. C. (1988). Curvature-compensated convective transport: SMART, A new boundedness-preserving transport algorithm. *International Journal for Numerical Methods in Fluids*, *8*(6), 617–641. http://dx.doi.org/10.1002/fld.1650080602

Guo, Y., Wu, C.-Y., & Thornton, C. (2013). Modeling gas-particle two-phase flows with complex and moving boundaries using DEM-CFD with an immersed boundary method. *AIChE Journal*, *59*(4), 1075–1087. http://dx.doi.org/10.1002/aic.13900

He, Y., Wang, T., Deen, N., van Sint Annaland, M., Kuipers, H., & Wen, D. (2012). Discrete particle modeling of granular temperature distribution in a bubbling fluidized bed. *Particuology*, *10*(4), 428–437. http://dx.doi.org/10.1016/j.partic.2012.02.001

Holland, D. J., Müller, C. R., Dennis, J. S., Gladden, L. F., & Sederman, A. J. (2008). Spatially resolved measurement of anisotropic granular temperature in gas-fluidized beds. *Powder Technology*, *182*(2), 171–181. http://dx.doi.org/10.1016/j.powtec.2007.06.030

Hoomans, B. P. B., Kuipers, J. A. M., Briels, W. J., & Van Swaaij, W. P. M. (1996). Discrete particle simulation of bubble and slug formation in a two-dimensional gas-fluidised bed: A hard-sphere approach. *Chemical Engineering Science*, *51*(1), 99–118.

Khawaja, H., Scott, S., Virk, M., & Moatamedi, M. (2012). Quantitative analysis of accuracy of voidage computations in CFD-DEM simulations. *Journal of Computational Multiphase Flows*, *4*(2), 183–192. http://dx.doi.org/10.1260/1757-482X.4.2.183

Kriebitzsch, S. H. L., van der Hoef, M. A., & Kuipers, J. A. M. (2013). Fully resolved simulation of a gas-fluidized bed: A critical test of DEM models. *Chemical Engineering Science*, *91*, 1–4. http://dx.doi.org/10.1016/j.ces.2012.12.038

Kuang, S. B., Yu, A. B., & Zou, Z. S. (2008). A new point-locating algorithm under three-dimensional hybrid meshes. *International Journal of Multiphase Flow*, *34*(11), 1023–1030. http://dx.doi.org/10.1016/j.ijmultiphaseflow.2008.06.007

Kuipers, J. A. M., Van Duin, K. J., Van Beckum, F. P. H., & Van Swaaij, W. P. M. (1993). Computer simulation of the hydrodynamics of a two-dimensional gas-fluidized bed. *Computers and Chemical Engineering*, *17*(8), 839–858.

Leonard, B. P. (1979). A stable and accurate convective modelling procedure based on quadratic upstream interpolation. *Computer Methods in Applied Mechanics and Engineering*, *19*(1), 59–98. http://dx.doi.org/10.1016/0045-7825(79)90034-3

Lim, E. W. C., Wang, C.-H., & Yu, A.-B. (2006). Discrete element simulation for pneumatic conveying of granular material. *AIChE Journal*, *52*(2), 496–509. http://dx.doi.org/10.1002/aic.10645

Liu, D., Bu, C., & Chen, X. (2013). Development and test of CFD–DEM model for complex geometry: A coupling algorithm for Fluent and DEM. *Computers and Chemical Engineering*, *58*, 260–268. http://dx.doi.org/10.1016/j.compchemeng.2013.07.006

Liu, D., Xiao, S., Chen, X., & Bu, C. (2012). Investigation of solid mixing mechanisms in a bubbling fluidized bed using a DEM-CFD approach. *Asia-Pacific Journal of Chemical Engineering*, *7*, S237–S244. http://dx.doi.org/10.1002/apj.553

Müller, C. R., Davidson, J. F., Dennis, J. S., Fennell, P. S., Gladden, L. F., Hayhurst, A. N., et al. (2007a). Oscillations in gas-fluidized beds: Ultra-fast magnetic resonance imaging and pressure sensor measurements. *Powder Technology*, *177*(2), 87–98. http://dx.doi.org/10.1016/j.powtec.2007.02.010

Müller, C. R., Davidson, J. F., Dennis, J. S., Fennell, P. S., Gladden, L. F., Hayhurst, A. N., et al. (2007b). Rise velocities of bubbles and slugs in gas-fluidised beds: Ultra-fast magnetic resonance imaging. *Chemical Engineering Science*, *62*(1–2), 82–93. http://dx.doi.org/10.1016/j.ces.2006.08.019

Müller, C. R., Holland, D. J., Sederman, A. J., Scott, S. A., Dennis, J. S., & Gladden, L. F. (2008). Granular temperature: Comparison of magnetic resonance measurements with discrete element model simulations. *Powder Technology*, *184*(2), 241–253. http://dx.doi.org/10.1016/j.powtec.2007.11.046

Müller, C. R., Scott, S. A., Holland, D. J., Clarke, B. C., Sederman, A. J., Dennis, J. S., et al. (2009). Validation of a discrete element model using magnetic resonance measurements. *Particuology*, *7*(4), 297–306. http://dx.doi.org/10.1016/j.partic.2009.04.002

Stewart, P. S. B., & Davidson, J. F. (1967). Slug flow in fluidised beds. *Powder Technology*, *1*(2), 61–80. http://dx.doi.org/10.1016/0032-5910(67)80014-7

Tagami, N., Mujumdar, A., & Horio, M. (2009). DEM simulation of polydisperse systems of particles in a fluidized bed. *Particuology*, *7*(1), 9–18. http://dx.doi.org/10.1016/j.partic.2008.11.008

Tsuji, Y., Kawaguchi, T., & Tanaka, T. (1993). Discrete particle simulation of two-dimensional fluidized bed. *Powder Technology*, *77*(1), 79–87.

Tsuji, Y., Tanaka, T., & Ishida, T. (1992). Lagrangian numerical simulation of plug flow of cohesionless particles in a horizontal pipe. *Powder Technology*, *71*(3), 239–250. http://dx.doi.org/10.1016/0032-5910(92)88030-L

Wu, C. L., Zhan, J. M., Li, Y. S., Lam, K. S., & Berrouk, A. S. (2009). Accurate void fraction calculation for three-dimensional discrete particle model on unstructured mesh. *Chemical Engineering Science*, *64*(6), 1260–1266. http://dx.doi.org/10.1016/j.ces.2008.11.014

Xiong, Q., Li, B., Zhou, G., Fang, X., Xu, J., & Wang, J. (2012). Large-scale DNS of gas–solid flows on Mole-8.5. *Chemical Engineering Science*, *71*, 422–430. http://dx.doi.org/10.1016/j.ces.2011.10.059

Zeilstra, C., van der Hoef, M. A., & Kuipers, J. A. M. (2008). Simulation of density segregation in vibrated beds. *Physical Review E*, *77*(3) http://dx.doi.org/10.1103/PhysRevE.77.031309